JOINT EUROPEAN TORUS

JET–P(91)50

D.P. O'Brien, L.L. Lao, E.R. Solano, M. Garribba, T.S. Taylor,
G. Cordey, J.J. Ellis and JET Team

Equilibrium Analysis of Iron-Core Tokamaks using a Full-Domain Method

Equilibrium Analysis of Iron-Core Tokamaks using a Full-Domain Method

D.P. O'Brien, L.L. Lao[1], E.R. Solano[2], M. Garribba, T.S. Taylor,
G. Cordey, J.J. Ellis and JET Team*

JET-Joint Undertaking, Culham Science Centre, OX14 3DB, Abingdon, UK

[1]General Atomics, San Diego, California, USA
[2]University of Texas, Austin
Work supported by US Department of Energy. Contract DE-AC03-89ER51114.
General Atomics Project 3466
** See Appendix 1*

Preprint of Paper to be submitted for publication in
Nuclear Fusion

ABSTRACT.

An efficient full-domain method for plasma equilibrium reconstruction in iron-core tokamaks is described. lllustrative calculations and comparison with results obtained from a finitedomain method using JET data are given. The results show that both types of methods are in agreement with respect to global plasma parameters such as stored energy, internal inductance, volume, and edge safety factor. However, when there is an uncertainty in the magnetic flux loop measurements, the full-domain method yields a more accurate separatrix location.

1. INTRODUCTION

In the operation of a tokamak, equilibrium analysis using magnetic data is an essential part of data analysis. An accurate description of the magnetic equilibrium is needed to interpret information from most other diagnostics, and for further investigations such as plasma confinement, transport studies and MHD stability analysis. Many working tokamaks use an inductor with a ferromagnet iron core to excite and sustain the plasma current in order to reduce the energy required to power the electromagnetic system of the inductor. However, the presence of a medium with the magnetic permeability $\mu_r \equiv \mu_0 >> 1$ near the plasma distorts the configuration of the magnetic field which holds the plasma in equilibrium, changes the shape of the plasma boundary and substantially affects the plasma equilibrium. The influence of the iron core can be difficult to include in equilibrium reconstruction due to the sometimes complicated geometrical and magnetic properties of the core. In the limiting cases when the conditions of high μ_r apply, the influence of the core on the equilibrium can be taken into account in a relatively simple way by imposing the boundary condition of vanishing tangential component of the poloidal magnetic field at the iron/air interface. This approximation breaks down if the magnetic induction of the core is large enough to saturate the permeability function.

Finite domain methods of equilibrium reconstruction avoid the problems of the iron core by solving a free boundary equilibrium problem inside a region defined by the flux measurements [1-3]. These methods have been developed extensively but suffer from needing a complete and very accurate knowledge of the magnetic flux at the boundary, which can make results sensitive to errors in flux measurements, particularly when there is a separatrix nearby.

We report here a full domain method to solve the plasma equilibrium analysis problem in the presence of an iron core. The method applies quite generally, independent of the complicated geometrical or non-linear magnetic properties of the core. It is an extension of a method proposed earlier for air core tokamaks [4,5]. The complex geometry of the iron core is properly treated by imposing a number of constraints on the tangential component of the poloidal magnetic field around the iron core boundary, which self-consistently take into account the magnetization current inside the core. The optimization problem is then solved by inverting the Grad-Shafranov equation while approximately conserving the externally measured magnetic fluxes and field, as well as other constraints imposed.

To test the applicability of the full domain method two kinds of benchmark calculations were performed. In the first test, reconstructive calculations were done using simulated signals generated by the equilibrium code PROTEUS [6]. The results from the reconstruction were then compared to the initial equilibrium values. In the second test, the equilibria of JET discharges were reconstructed from external magnetic data and the results obtained using this new method were compared to those from the IDENT code [3], which is based on a finite domain method and is presently in routine use at JET.

In Section 2, a brief summary of the theoretical model and the method used to reconstruct the equilibria from the experimental measured magnetic data is presented. In Section 3, the results of the analysis using JET experimental data are discussed. Finally, a summary is given in Section 4.

2. SUMMARY OF THEORETICAL METHOD

2.1 MHD equilibrium

The pertinent elements of the JET device are illustrated in Figs 1a and 1b. The relevant toroidal currents are those of the plasma inside the vacuum vessel and the Ohmic and shaping coil currents, together with the magnetization currents in the iron core.

The usual representation of the axisymmetric magnetic field $\bar{B}$ is used, where $\bar{B}$ is represented in terms of two scalar functions ψ and F, describing the poloidal magnetic flux per radian of the toroidal angle ϕ and the poloidal current enclosed between a flux surface and the central symmetric axis, respectively

$$\bar{B} = \bar{\nabla}\psi \times \bar{\nabla}\phi + \frac{\mu_o F}{2\pi}\bar{\nabla}\phi \quad , \tag{1}$$

and R is the distance from the axis of symmetry. The Grad-Shafranov equation for the equilibrium is, using the usual (R, ϕ, Z) cylindrical coordinates,

$$\Delta^* \psi = -\mu_o R J_T \quad , \tag{2}$$

$$J_T = R\left[P'(\psi) + \frac{\mu_o F F'(\psi)}{4\pi^2 R^2}\right]G + J_C + J_I \quad , \tag{3}$$

$$\Delta^* = \frac{\partial^2}{\partial R^2} - \frac{1}{R}\left(\frac{\partial}{\partial R}\right) + \frac{\partial^2}{\partial Z^2} \quad , \tag{4}$$

where Z is the coordinate in the vertical direction, P is the plasma pressure, and J_T is the toroidal current density. The latter consists of currents flowing in the Ohmic and the shaping coils, J_C, in the iron core structure, J_I, as well as in the plasma region represented by the term involving G defined by

$$G(R, Z) = \begin{cases} 1, \text{ if } (R,Z) \text{ inside vacuum vessel and limiter;} \\ 0, \text{ otherwise.} \end{cases} \tag{5}$$

The boundary condition for Eq. (2) is $\psi = 0$ at R = 0 and at infinity.

The toroidal currents in the Ohmic and the shaping coils, J_C, are known experimentally, whereas the toroidal iron core currents, J_I, are not. They are modelled

as currents flowing in N coils. The cross sectional area of these coils are chosen to match the geometry of the iron core transformer, as illustrated in Fig. 1b. Inside the cross sectional area of each coil the current density is taken to be uniform. Thus, the iron core currents are described by N parameters, which are then determined by matching to the measured magnetic data, and the constraints imposed on the tangential component of the poloidal magnetic field around the iron-core boundary which self consistently takes into account its permeability as described in section 2.3.

2.2 Representation of the plasma current

The equilibrium constraint relates the toroidal current density J_T to the pressure P and the poloidal current F and permits a reduction of the dimensionality of the reconstruction problem by expressing the two-dimensional function J_T in terms of two one-dimensional free functions, P and F. These functions are unfolded from the measured data, by representing them in terms of a number of parameters, α_n and γ_n which are determined by fitting to the available data. Additionally the two free functions are parameterized linearly in terms of α_n and γ_n using the basis functions x_n:

$$P'(\psi) = \sum_{n=0}^{np} \alpha_n x_n, \tag{6}$$

$$FF'(\psi) = \sum_{n=0}^{n_F} \gamma_n x_n \tag{7}$$

Many choices of the basis functions x_n to represent P and F are possible. Here, the polynomial set $x_n = x^n$ is used, where $x = (\psi - \psi_0)/(\psi - \psi_0)$ is the normalized poloidal flux enclosed by a particular flux surface, and ψ_b and ψ_0 are the poloidal flux at the plasma boundary and that at the magnetic axis, respectively. The number of parameters n_P and n_F that can be determined depends critically on the amount of the experimental data available as well as on the accuracy of the data, as described in detail in Refs. 4 and 5.

2.3 Representation of the iron core current

The JET iron core is described in Refs. [3] and [7]. As with many other tokamak iron core transformers it is inherently a three dimensional structure. It has eight sections, one to each octant of JET. Each section consists of an inner solenoidal core with return limbs as shown in Fig. 1a. To facilitate the analysis we take an equivalent axisymmetric two dimensional model of the core as described in Ref. [7]. The poloidal cross-section of the two dimensional equivalent structure is shown in Fig. 1a. The core currents are taken as surface currents which flow in N sections of the iron. Each section

has a uniform current, and is further split into a sufficient number of smaller segments to give an accurate description of the geometry in the numerical evaluation of the inductance matrix.

The boundary conditions at the iron-air interface of a segment i is that the poloidal flux ψ and the tangential component of the magnetic intensity are continuous across the interface Γ_i

$$\psi^{iron}(\Gamma_i) = \psi^{air}(\Gamma_i) \tag{8}$$

$$B_t^{iron}(\Gamma_i) = \mu_r(B_i) B_t^{air}(\Gamma_i) \tag{9}$$

where μ_r is the relative permeability of the iron-core segment i. Equation (9) can be rewritten in terms of the total surface magnetization currents, I_{mi}, in the iron-core segment i, and the tangential poloidal magnetic fields, B_t^e, due to the plasma, the shaping, and the ohmic coils as [8 - 10]

$$\left[\mu_r(B_i)-1\right]\left[B_t^e(\Gamma_i)+\sum_{j=i} G_B(\Gamma_i,\Gamma_j)\, I_{mj}\right] - \left[\mu_r(B_i)+1\right]\frac{\mu_o I_{mi}}{2L_i} = 0 \tag{10}$$

where $G_B(\Gamma_i, \Gamma_j)$ is the inductance matrix relating the tangential poloidal magnetic field at iron-core segment Γ_i to the magnetization current I_{mj} flowing in segment Γ_j, and L_i is the length of iron-core segment i.

If an experimental look-up table is available for the permeability μ_r, as a function of the magnetic induction B, Eq. (10) together with the relevant external magnetic measurements provide a set of constraints for the determination of the magnetization current I_{mi}. This is achieved using an iterative process to force the consistency between the local values of B_i at the core segments, the surface magnetization currents I_{mi}, and the permeability function $\mu_r(B_i)$.

For an unsaturated iron-core segment with $\mu_r >> 1$, Eqs. (9) and (10) reduce simply to the boundary condition that the tangential component of the poloidal magnetic field vanishes at the interface. This assumption is valid for many outer sections of the transformer at JET during the whole of a discharge. This boundary condition is conveniently implemented by placing a set of simulated tangential poloidal magnetic probes at selected positions around the transformer, as shown in Fig. 1b, and requiring the tangential probe signal at this section to be zero in the fitting.

The inner solenoid of the core however has finite permeability. If any section of it is completely saturated ($\mu_r \sim 1$), we may take the surface current in that section to be zero as shown in Eq. (10). In the rest of this paper, we will concentrate the discussion on the cases when the magnetization currents in the core segments which have finite permeability are determined from the appropriate external magnetic measurements. The magnetization currents, I_{mi}, in these segments are free parameters, which are in addition to the parameters describing the plasma current profile. This has the advantage that the results do not depend on the accuracy of the permeability table. However, the number N of the core sections is restricted by the number of available magnetic measurements. The use of the look up permeability table in the analysis will be described separately in a future report.

2.4 Determination of current profile parameters

The non-linear optimization problem is solved using an enhanced version of the EFIT code EFITJ. The method is described in detail in Ref. [4]. Briefly, the Grad-Shafranov Eq. (2) is solved by inverting the Δ^* operator while approximately conserving the externally measured and simulated poloidal magnetic fluxes and fields through minimizing

$$\chi^2 = \sum_{j=1}^{n_M} \left(\frac{M_j - C_j}{\sigma_j} \right)^2 \quad , \tag{11}$$

where C_j and σ_j are the computed values and the uncertainty of the corresponding measured and simulated quantities M_j, respectively, and n_M is the total number of all the data used. If the minimum of χ^2 equals the difference between the number of independent measurements and the number of adjustable parameters, the fit is good and there is no justification for introducing more adjustable parameters.

This minimisation problem is non-linear and can be computationally very intensive if a conventional optimization approach is adopted. Here, it is efficiently solved, using a well developed previous approach by transforming it into a sequence of linearised optimization problems interleaved with the equilibrium calculations using the Picard iteration scheme, as described in detail in Ref. [4].

3. BENCHMARK CALCULATIONS

To demonstrate the capability of this method to accurately reconstruct plasma equilibria from the available magnetic signals various tests have been performed. Detailed comparative calculations using the JET configurations are given in this section. The magnetic diagnostics of JET used in the calculations are shown in Fig. 1b. They consist of 14 saddle loops, and a maximum of 34 magnetic probes. There are 10 external poloidal shaping coils. There are additionally the M simulated tangential probes which are placed at each iron core section, some of which may be used in the fitting to impose the constraints of zero tangential poloidal magnetic field. If any section of the core may be assumed saturated then zero current may be placed in this section and used in the fitting. The iron core is devided into 24 segments. The following comparisons are made:

3.1 Solovev equilibrium

The results of a Solovev equilibrium [11] computed using EFITJ are compared against the known analytic results. These are shown in Fig. 2 where the solid lines represent the numerical solutions using EFITJ whereas the dashed lines represent the exact analytic results. The results from EFITJ agree well with the exact analytic results. The maximum relative error of the poloidal flux inside the plasma being less than 1%.

3.2 Self-consistency check

We show sufficiency of the available magnetic probes by giving a self consistent reconstruction of a limiter equilibrium and a divertor equilibrium. The equilibrium is generated by performing a fixed boundary calculation using EFITJ, where the plasma shape is specified as consisting of a finite number of thin flux loops which have equal flux values along the designated plasma boundary. Once this fixed boundary calculation has been performed the signals at the location of the available probes are simulated using the calculated equilibrium. A free boundary reconstruction is then performed using EFITJ and the results compared with those of the original fixed boundary calculation. The results of the comparison are shown in Figs. 3a and b. The two results agree well with each other. The solid lines represent the results from the free boundary reconstruction, whereas the dashed lines represent the results from the fixed boundary calculation.

3.3 Comparison against PROTEUS

In the third test we examine the accuracy of our iron core model by reconstructing an equilibrium generated by the standard predictive equilibrium code PROTEUS [6]. PROTEUS is a 2-D finite element code describing the time evolution of a plasma and of the external field on the resistive time scale in toroidal axisymmetric configurations.

This code uses a model of the JET iron core built in through a given permeability function and self-consistently includes the external poloidal field circuits. The signals at the probes are taken from PROTEUS, which are then used as input in the EFITJ calculations to reconstruct the equilibrium. Two kinds of tests were performed. In the first test, we consider a vacuum case where the plasma is absent. From the flux loop signals and the boundary constraints of zero tangential poloidal magnetic field at the unsaturated outer segments, the magnetization currents are determined. The signals at the magnetic probes are then computed and compared with those from PROTEUS. The results are summarized in Fig. 4. We see that the predicted magnetic probe signals from EFITJ (solid curves) agree well with those from PROTEUS (solid circles).

In the second test, we consider a full reconstruction with the plasma present. From the flux loop and magnetic probe signals given by PROTEUS, a double null equilibrium is reconstructed. The results are summarized in Figs. 5a - 5e, showing that the results from EFITJ agree well with those from PROTEUS.

4. ANALYSIS OF JET MAGNETIC DATA

For the analysis of JET experimental data we consider a double null 2 MA high β shot 20272. The major plasma parameters for this discharge near the peak β time of 52.5s are given Table 1. In Figs. 6a - 6d, the calculated results from EFITJ are compared with the experimental signals. We see that the fit to both the flux and magnetic field measurements is extremely good. The time trace of the most important global parameters are shown in Figs. 7a - 7d, and a comparison made with the finite domain code IDENT [3]. We see that for the stored energy, plasma volume the major radius and vertical position of the magnetic axis, there is good agreement, which lies well within the margins set by experimental error. The plasma boundaries derived from the two methods are compared in Fig. 8. The agreement is seen to be good everywhere except possibly in the vicinity of the X-points. In Fig. 9 the X-point location is compared between the two codes and that of a local expansion technique used routinely at JET [11]. We see that there is excellent agreement between EFITJ and the local expansion results while the finite domain code shows a disagreement. This difference is due to the reconstruction method used in the finite domain code IDENT, which uses the measured flux loop signals as boundary conditions in the reconstruction without taking into account properly the measurement errors in the flux. Thus, when there is a separatrix near the boundary of the computational domain defined by the flux loop measurements, the reconstructed separatrix location can have a large uncertainty.

5. SUMMARY

From the results of this study, it can be concluded that the full domain equilibrium reconstruction method developed here gives an accurate and full description of tokamak plasmas with an iron core transformer. Comparisons with a finite domain method show good agreement. The advantage of the full domain method is that all the experimentally measured magnetic quantities available are fully utilized with their appropriate uncertainties in the fitting. In addition the fluxes are not absolutely conserved so that any experimental errors are properly treated in the fitting.

ACKNOWLEDGEMENTS

The authors thank P. Stubberfield and J.P. Christiansen for supplying some of the data and for valuable discussions, and V. Chan, R.S. Stambaugh and M. Keilhacker for their support. This is a report of work sponsored by the U.S. Department of Energy under Contracts No. DE-AC03-89ER51114.

REFERENCES

[1] BLUM, J., Le FOLL, J., THOORIS, B. Comput. Phys. Commun. 24 (1981) 235.

[2] LAZZARO, E., MANTICA, P., Nucl. Fusion 28 (1988) 913.

[3] BRUSATI, M., CHRISTIANSEN, J.P., CORDEY, J.G., JARRETT, K., LAZZARO, E., ROSS, R.T., Comput. Phys. Rep. 1 (1984) 345.

[4] LAO, L.L., St JOHN, H., STAMBAUGH, R.D., KELLMAN, A.G., PFEIFFER, W., Nucl. Fusion **25** (1985) 1611.

[5] LAO, L.L., FERRON, J.R., GROEBNER, R.J., HOWL, W., St. JOHN, H., STRAIT, E.J., TAYLOR, T.S., Nucl. Fusion 30 (1990) 1035.

[6] R. ALBAWESE, J., BLUOR and O. DE BARBIERI, "The PROTEUS code", presented at the workshop on "Feedback Systems for Shape Control of Non-Circular Tokamaks", Lausanne, Switzerland, July 13-17, 1987.

[7] KHALAFALLAH, A.K., LAST, J.R., BREWIN, D.T., THOMAS, C., JET Technical Note JTN/E 61 (1970)

[8] GRYAZNEVICH, M.P., KILOVATAYA, T.G., PYATOV, V.N., Sov. J. Plasma Phys. 9 (1983) 414.

[9] ZAKHAROV, L.F., SHAFRANOV, V.D., Reviews of Plasma Physics, Vol 11, (M.A. LEONTOVICH, Ed.), Consultants Bureau, New York (1986).

[10] ATANASIU, C.V., ZAKHAROV, L.E. Nucl. Fusion 30 (1990) 1027.

[11] SOLOVEV, L.S., Sov. Phys. JET P 26 (1968) 400.

[12] O'BRIEN, D.P., et al., 17th Eur. Conf. Contr. Fusion Plasma Heating, Amsterdam, ECA 14B part 1 (1990), 251.

TABLE I. MAJOR PLASMA PARAMETERS
FOR JET SHOT 20272 AT t = 52.50 secs.

Major radius, R_o	3.14 m
Minor radius, a	1.12 m
Elongation, κ	1.82
Upper triangularity, δ_U	0.43
Lower triangularity, δ_L	0.43
Toroidal beta, $\bar{\beta}_T$	4.0%
Poloidal beta, $\bar{\beta}_P$	0.68
Internal inductance, ℓ_i	0.83
q_{95}	4.5
I_p	2.08 MA
B_T	1.2 T

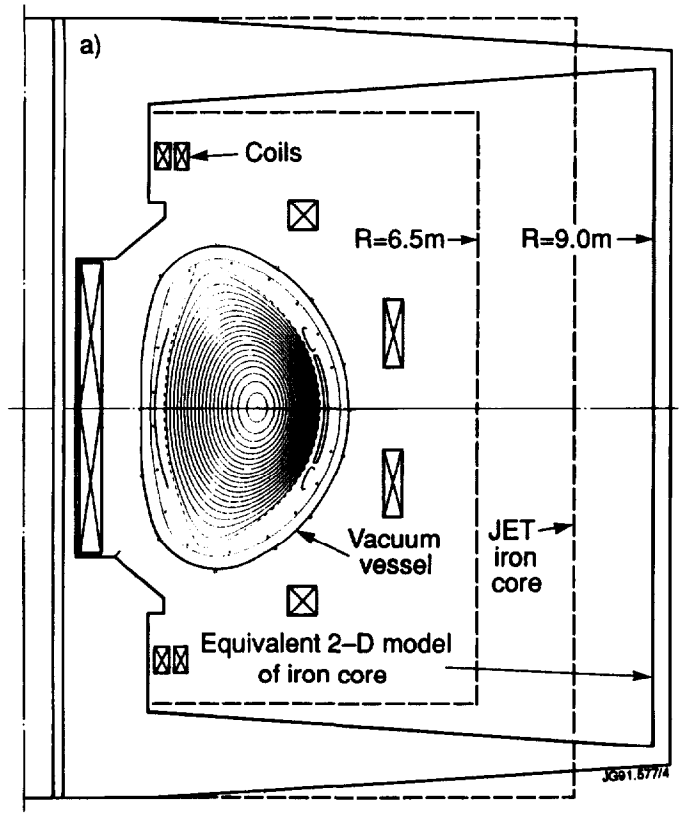

FIG. 1a. A cross section of the JET device, showing the locations of the coils, the vacuum vessel, the JET iron-core and the equivalent 2-D iron-core transformer.

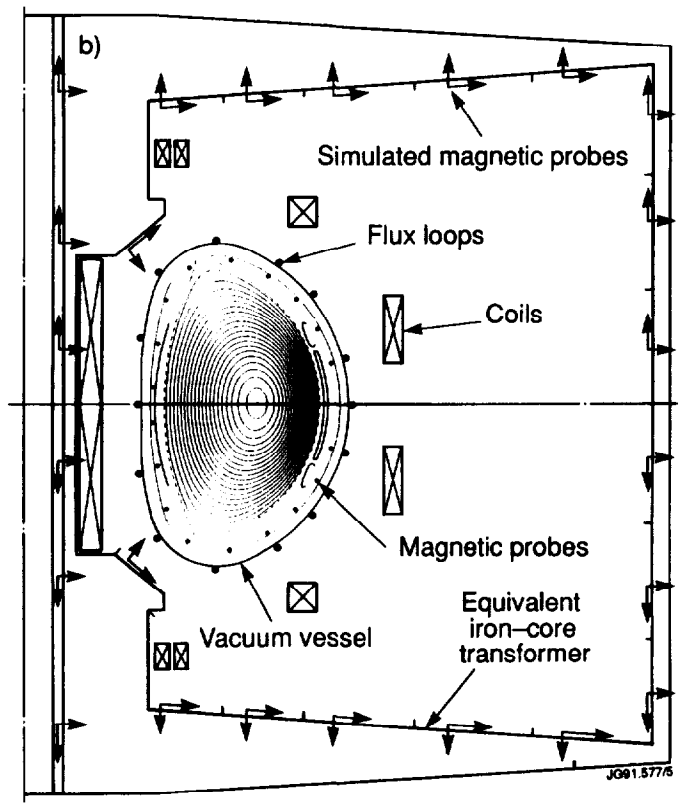

FIG. 1b. A cross section of the JET device showing the locations of the Ohmic heating coils, the magnetization coils, the shaping coils, the vacuum vessel, the flux loops, the magnetic probes and the iron-core transformer.

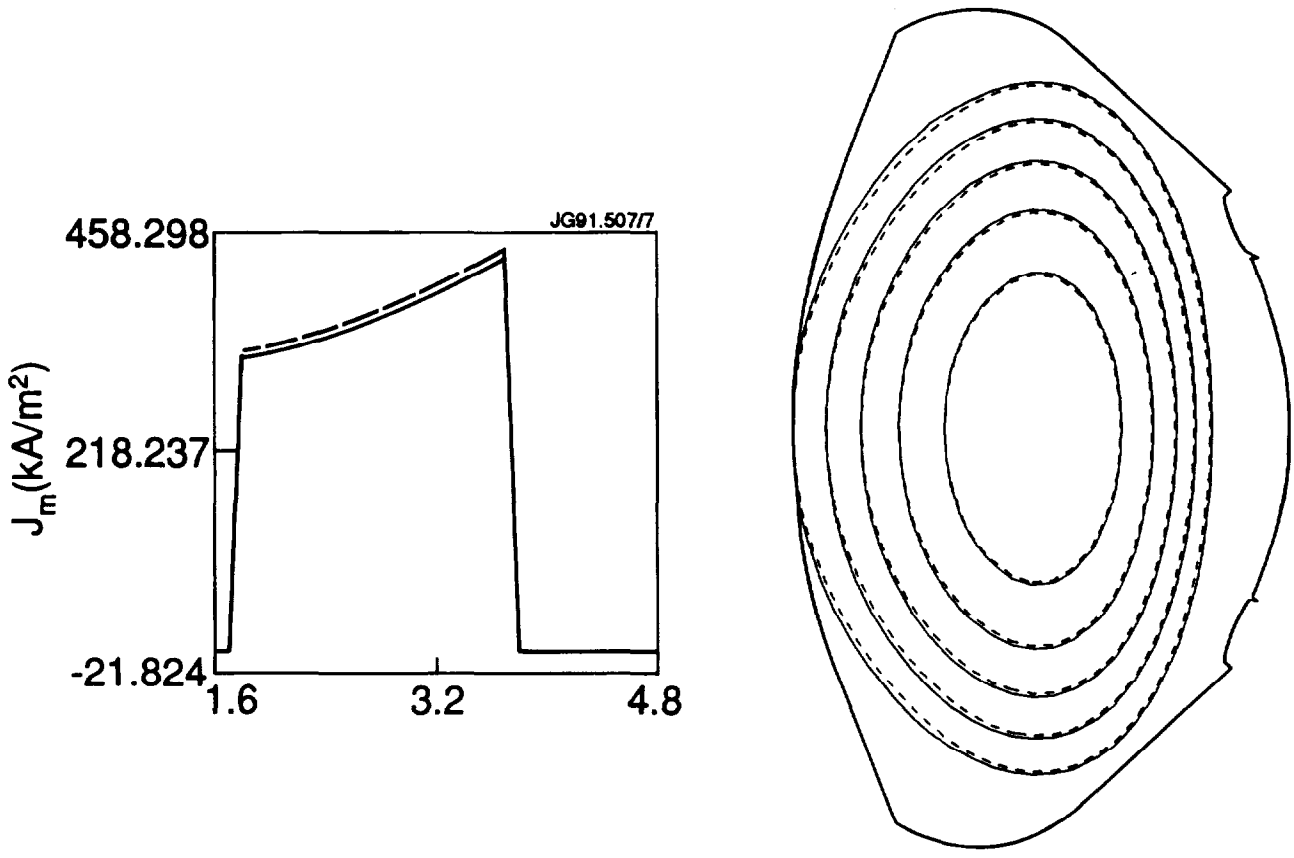

FIG. 2. Comparison of numerical results (solid curves) to analytical Solovev solution (dashed curves). J_m is the toroidal current density across the horizontal plane passing through the magnetic axis.

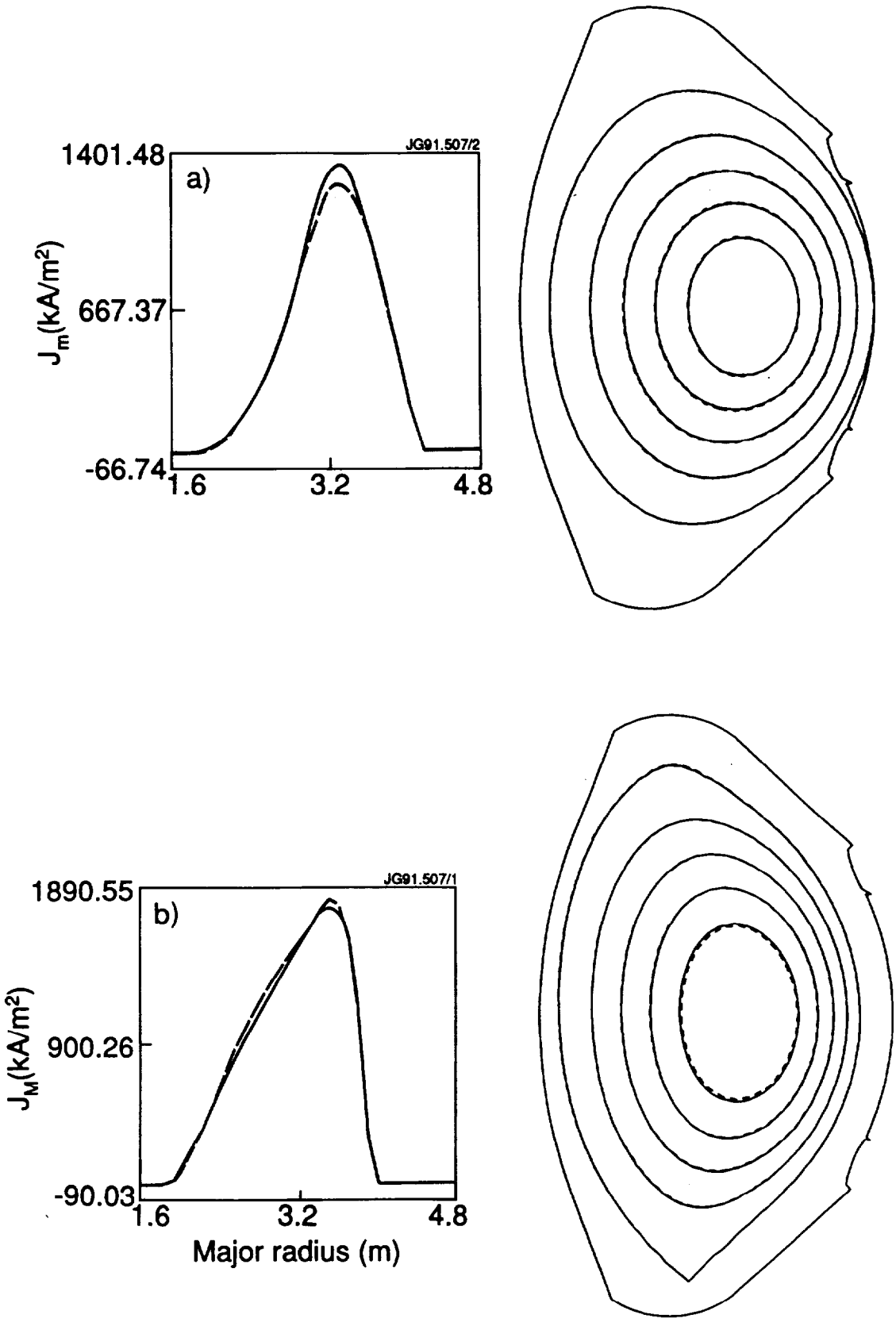

FIG. 3. Comparison of reconstruction results (solid curves) to initial equilibrium results (dashed curves). J_m is the toroidal current density across the horizontal plane passing through the magentic axis. a) Limiter Configuration b) Divertor Configuration.

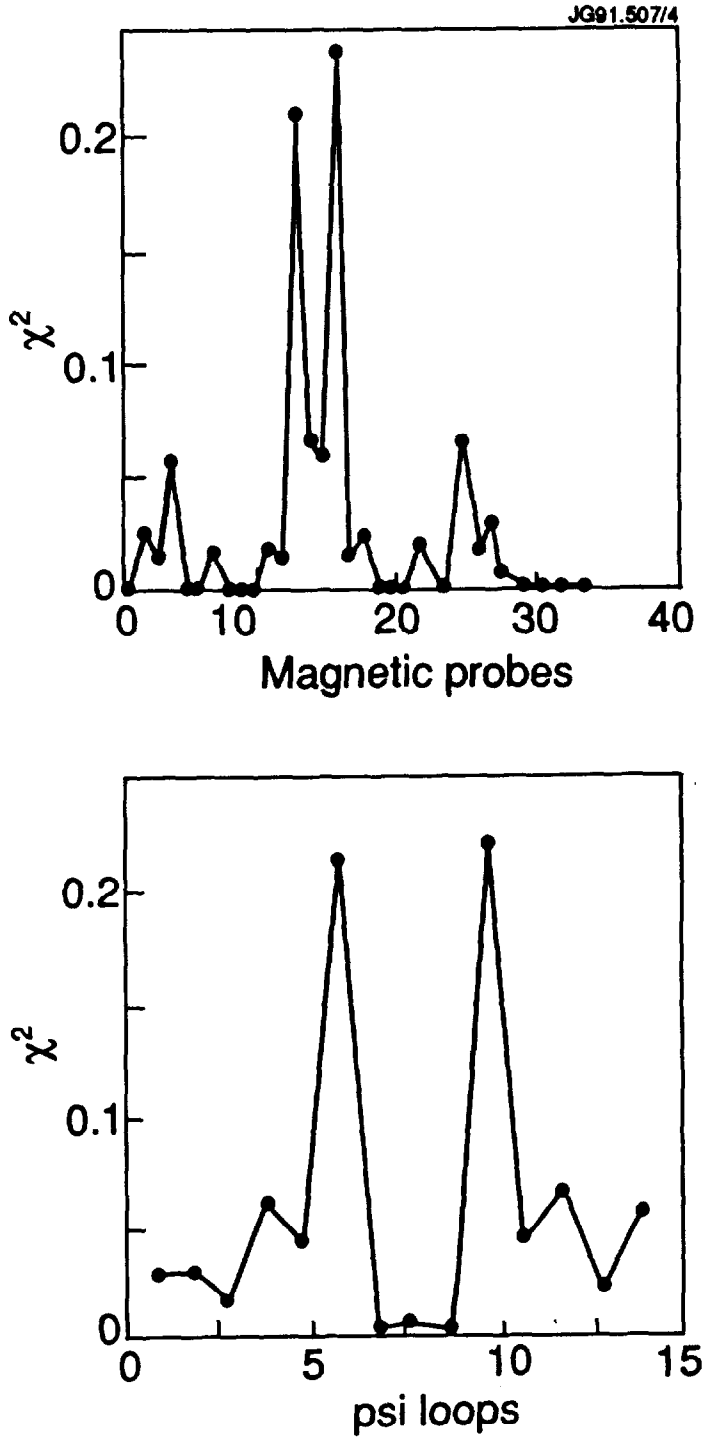

FIG. 4. Comparison of EFITJ results (solid curves) to PROTEUS results (solid circles) for a vacuum case.

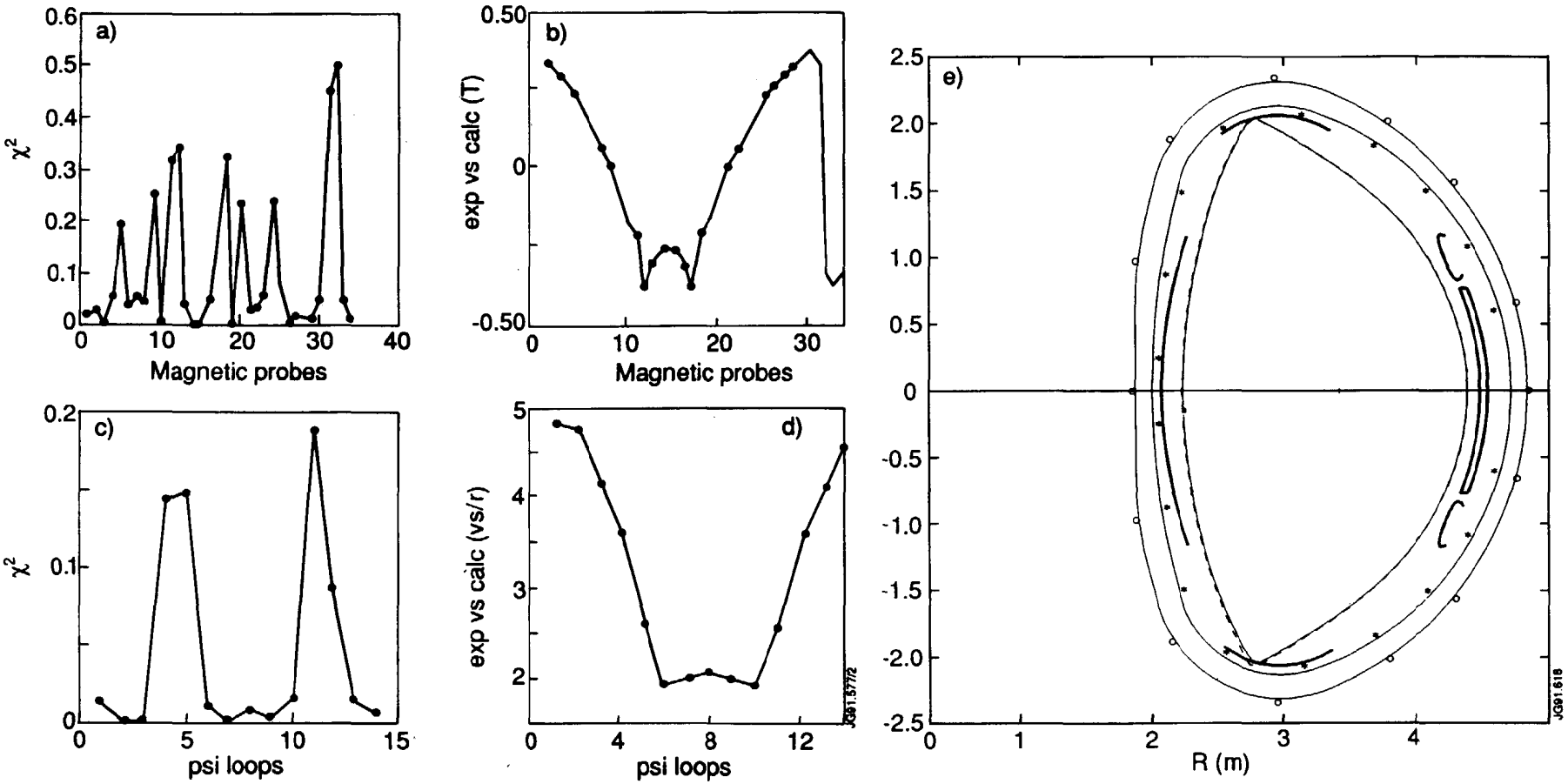

FIG. 5. Comparison of EFITJ results (solid curves) to PROTEUS results (solid circles) for a plasma case. a,b) χ^2 and comparison for the magnetic probes c,d) χ^2 and comparison for the flux loops e) Plasma boundaries derived from Proteus (solid) and EFIT (dashed).

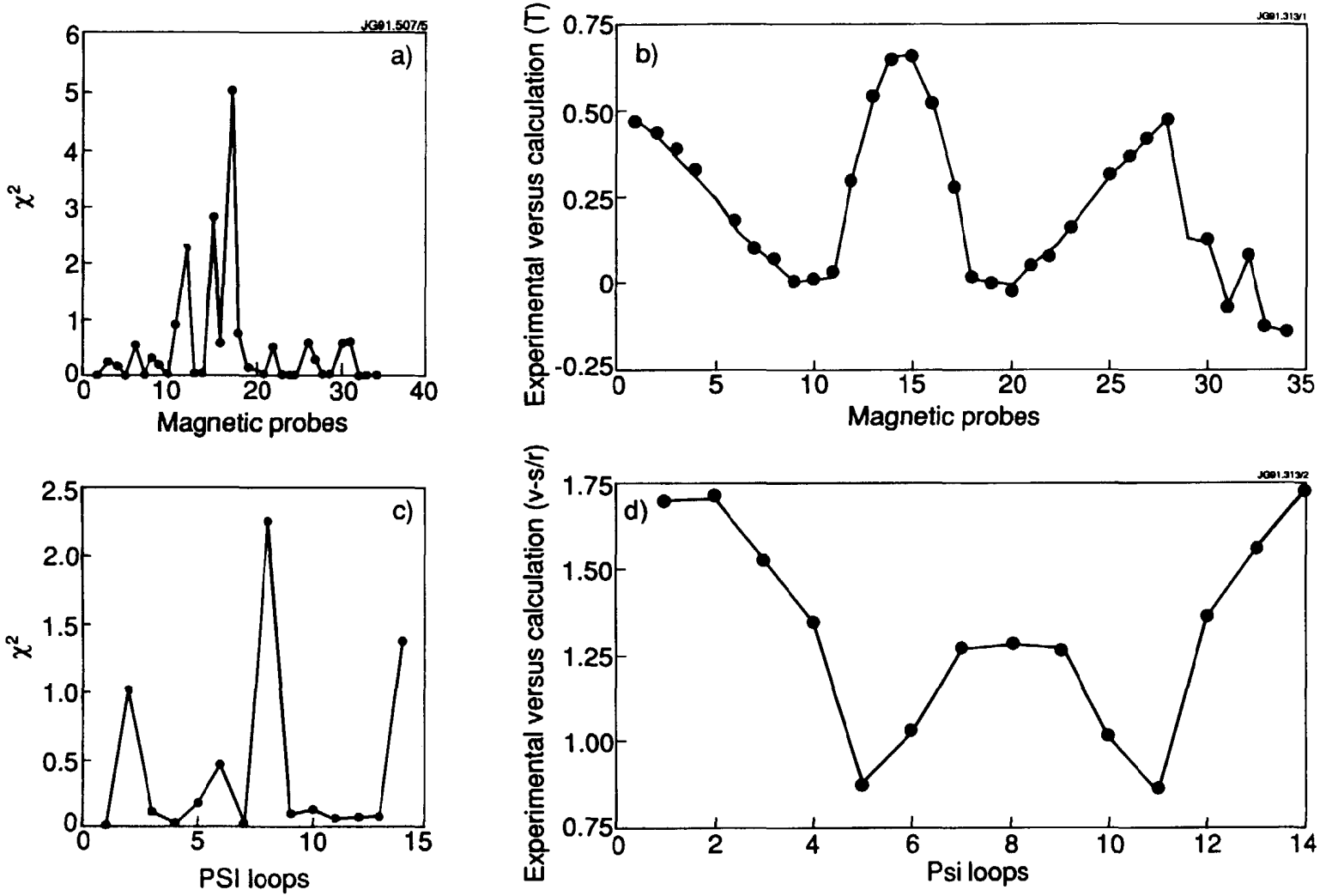

FIG. 6. Comparison of EFITJ reconstruction results (solid curves) for JET discharge 20272 against experimental results (solid circles). a,b) χ^2 and comparison for the magnetic probes c,d) χ^2 and comparison for the flux loops.

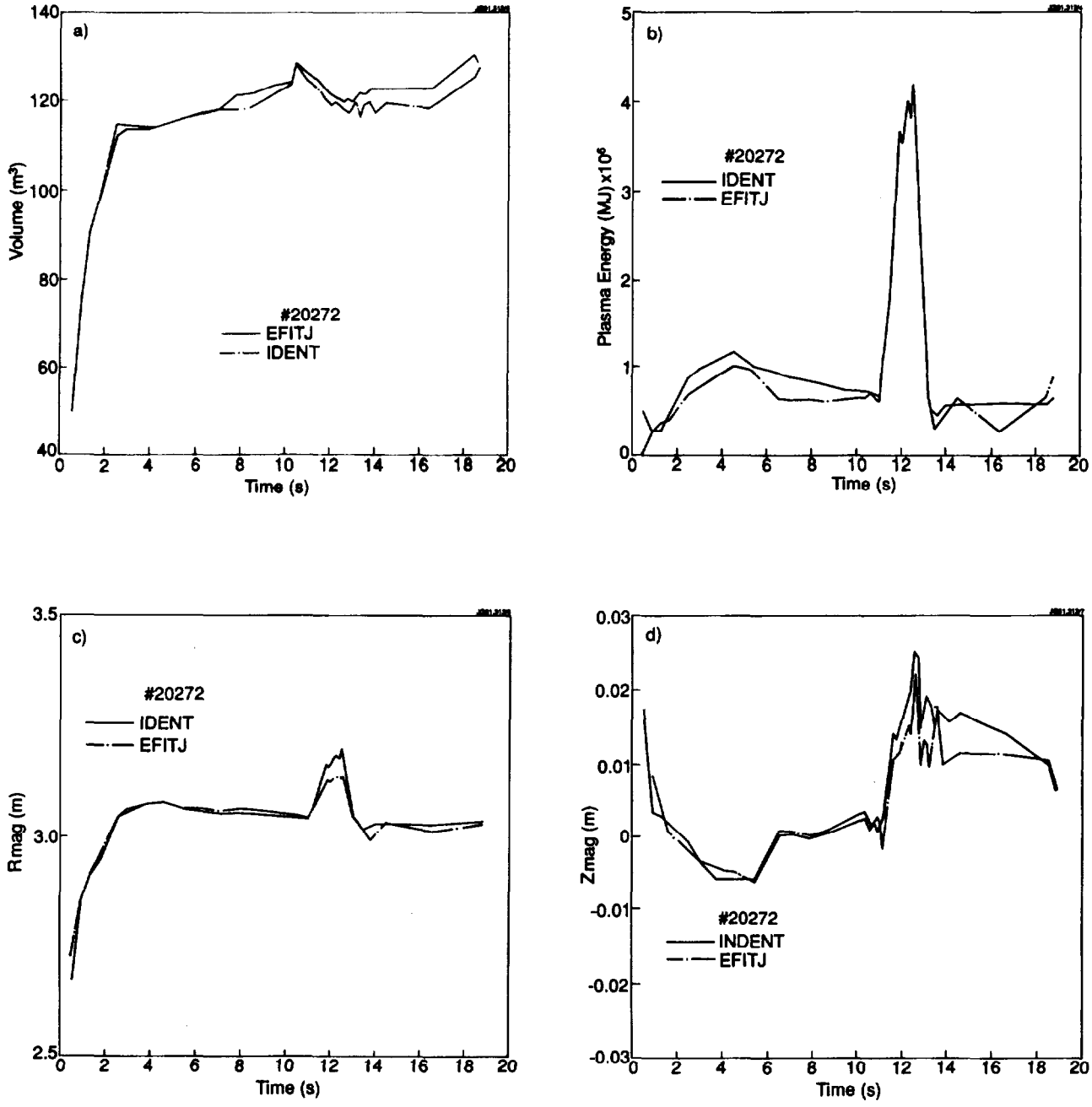

FIG. 7. Comparison of EFITJ reconstruction results for JET discharge 20272 against results from IDENT. a) Plasma Volume b) Plasma Energy c) Major Radius of Magnetic Axis d) Z coordinate of the magnetic axis.

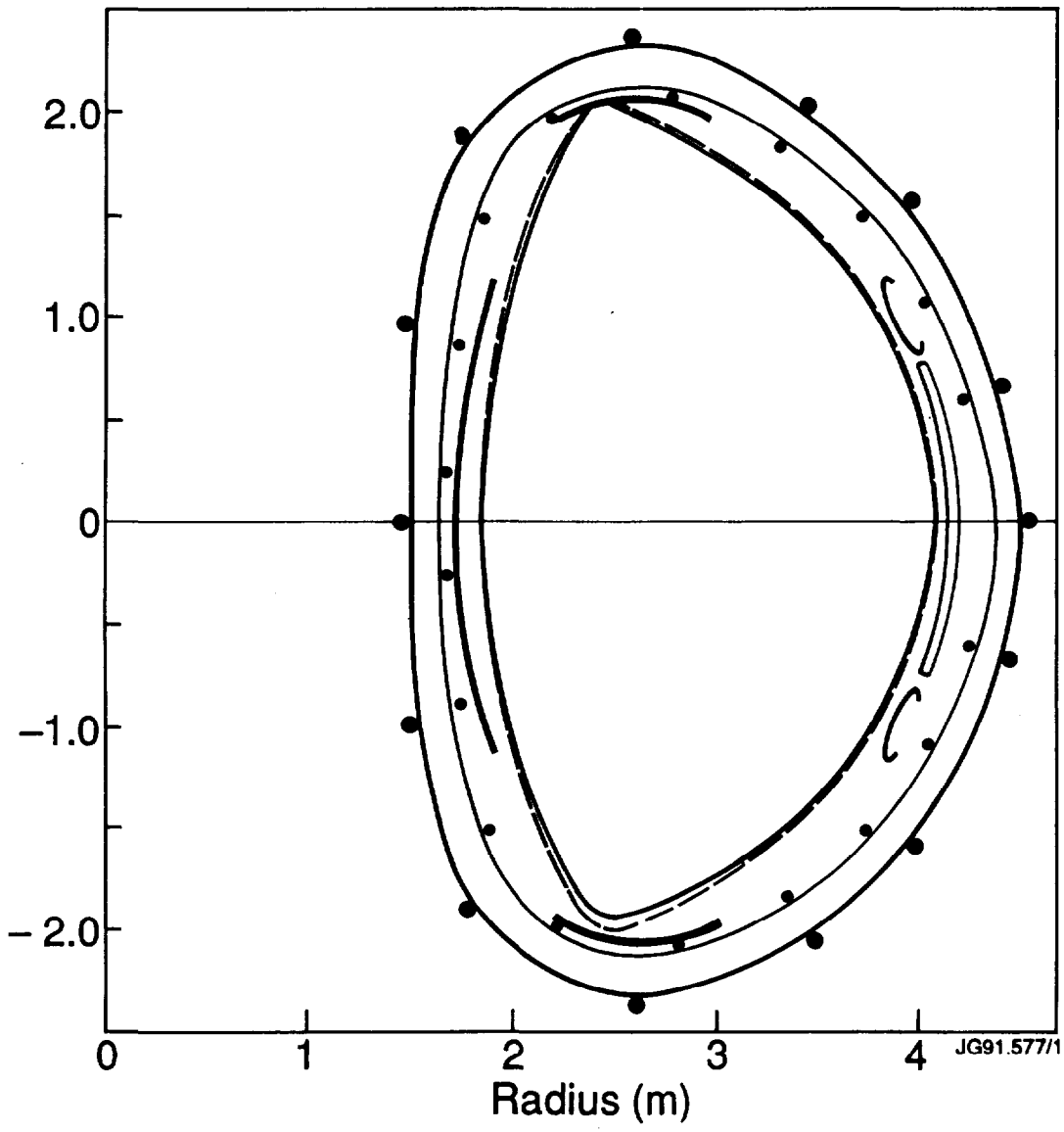

Fig. 8. Comparison of Plasma Boundaries derived from IDENT (solid) and EFITJ (dashed).

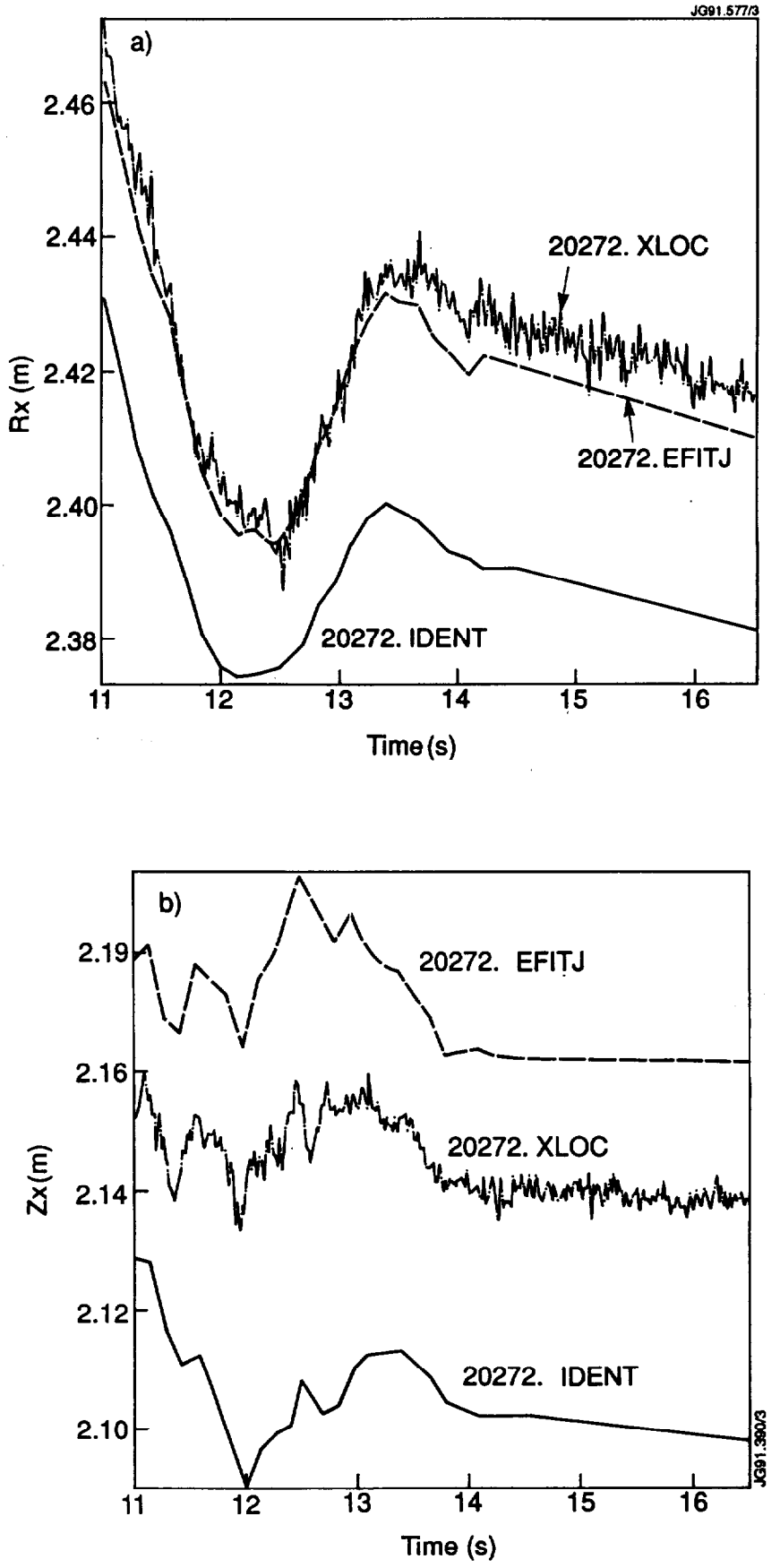

FIG. 9. Comparison of EFITJ reconstruction results of the separatrix location for JET discharges 20272 against results from IDENT and XLOC. a) major radius of upper X-point b) Z coordinate of upper X-point.

Appendix I

THE JET TEAM

JET Joint Undertaking, Abingdon, Oxon, OX14 3EA, U.K.

J.M. Adams[1], H. Altmann, A. Andersen[14], P. Andrew[18], M. Angelone[29], S.A. Arshad, W. Bailey, P. Ballantyne, B. Balet, P. Barabaschi, R. Barnsley[2], M. Baronian, D.V. Bartlett, A.C. Bell, I. Benfatto[5], G. Benali, H. Bergsaker[11], P. Bertoldi, E. Bertolini, V. Bhatnagar, A.J. Bickley, H. Bindslev[14], T. Bonicelli, S.J. Booth, G. Bosia, M. Botman, D. Boucher, P. Boucquey, P. Breger, H. Brelen, H. Brinkschulte, T. Brown, M. Brusati, T. Budd, M. Bures, T. Businaro, P. Butcher, H. Buttgereit, C. Caldwell-Nichols, D.J. Campbell, P. Card, G. Celentano, C.D. Challis, A.V.Chankin[23], D. Chiron, J. Christiansen, C. Christodoulopoulos, P. Chuilon, R. Claesen, S. Clement, E. Clipsham, J.P. Coad, M. Comiskey[4], S. Conroy, M. Cooke, S. Cooper, J.G. Cordey, W. Core, G. Corrigan, S. Corti, A.E. Costley, G. Cottrell, M. Cox[7], P. Cripwell, H. de Blank[15], H. de Esch, L. de Kock, E. Deksnis, G.B. Denne-Hinnov, G. Deschamps, K.J. Dietz, S.L. Dmitrenko, J. Dobbing, N. Dolgetta, S.E. Dorling, P.G. Doyle, D.F. Düchs, H. Duquenoy, A. Edwards, J. Ehrenberg, A. Ekedahl, T. Elevant[11], S.K. Erents[7], L.G. Eriksson, H. Fajemirokun[12], H. Falter, D. Flory, J. Freiling[15], C. Froger, P. Froissard, K. Fullard, M. Gadeberg, A. Galetsas, D. Gambier, M. Garribba, P. Gaze, R. Giannella, A. Gibson, R.D. Gill, A. Girard, A. Gondhalekar, C. Gormezano, N.A. Gottardi, C. Gowers, B.J. Green, R. Haange, G Haas, A. Haigh, G. Hammett[6], C.J. Hancock, P.J. Harbour, N.C. Hawkes[7], P. Haynes[7], J.L. Hemmerich, T. Hender[7], F.B. Herzog, R.F. Herzog, J. Hoekzema, J. How, M. Huart, L Hughes, T.P. Hughes[4], M. Hugon, M. Huguet, A. Hwang[7], B. Ingram, M. Irving, J. Jacquinot, H. Jaeckel, J.F. Jaeger, G. Janeschitz[13], S. Jankowicz[22], O.N. Jarvis, F. Jensen, E.M. Jones, L.P.D.F. Jones, T.T.C. Jones, J-F. Junger, E. Junique, A. Kaye, B.E. Keen, M. Keilhacker, G.J. Kelly, W. Kerner, R. Konig, A. Konstantellos, M. Kovanen[20], G. Kramer[15], P. Kupschus, R. Lässer, J.R. Last, B. Laundy, L. Lauro-Taroni, K. Lawson[7], M. Lennholm, A. Loarte, R. Lobel, P. Lomas, M. Loughlin, C. Lowry, B. Macklin, G. Maddison[7], G. Magyar, W. Mandl[13], V. Marchese, F. Marcus, J. Mart, E. Martin, R. Martin-Solis[8], P. Massmann, G. McCracken[7], P. Meriguet, P. Miele, S.F. Mills, P. Millward, R. Mohanti[17], P.L. Mondino, A. Montvai[3], S. Moriyama[28], P. Morgan, H. Morsi, G. Murphy, M. Mynarends, R. Myrnäs[16], C. Nardone, F. Nave[21], G. Newbert, M. Newman, P. Nielsen, P. Noll, W. Obert, D. O'Brien, J. O'Rourke, R. Ostrom, M. Ottaviani, M. Pain, F. Paoletti, S. Papastergiou, D. Pasini, A. Peacock, N. Peacock[7], D. Pearson[12], R. Pepe de Silva, G. Perinic, C. Perry, M. Pick, R. Pitts[7], J. Plancoulaine, J-P. Poffé, F. Porcelli, L. Porte[19], R. Prentice, S. Puppin, S. Putvinsko[23], G. Radford[9], T. Raimondi, M.C. Ramos de Andrade, P-H. Rebut, R. Reichle, E. Righi, F. Rimini, D. Robinson[7], A. Rolfe, R.T. Ross, L. Rossi, R. Russ, P. Rutter, H.C. Sack, G. Sadler, G. Saibene, J.L. Salanave, G. Sanazzaro, A. Santagiustina, R. Sartori, C. Sborchia, P. Schild, M. Schmid, G. Schmidt[6], B. Schunke, S.M. Scott, A. Sibley, R. Simonini, A.C.C. Sips, P. Smeulders, R. Stankiewicz[27], M. Stamp, P. Stangeby[18], D.F. Start, C.A. Steed, D. Stork, P.E. Stott, T.E. Stringer, P. Stubberfield, D. Summers, H. Summers[19], L. Svensson, J.A. Tagle[21], A. Tanga, A. Taroni, A. Tesini, P.R. Thomas, E. Thompson, K. Thomsen, J.M. Todd, P. Trevalion, B. Tubbing, F. Tibone, E. Usselmann, H. van der Beken, G. Vlases, M. von Hellermann, T. Wade, C. Walker, R. Walton[6], D. Ward, M.L. Watkins, M.J. Watson, S. Weber[10], J. Wesson, T.J. Wijnands, J. Wilks, D. Wilson, T. Winkel, R. Wolf, B. Wolle[24], D. Wong, C. Woodward, Y. Wu[25], M. Wykes, I.D. Young, L. Zannelli, Y. Zhu[26], W. Zwingmann.

PERMANENT ADDRESSES

1. UKAEA, Harwell, Didcot, Oxon, UK.
2. University of Leicester, Leicester, UK.
3. Central Research Institute for Physics, Academy of Sciences, Budapest, Hungary.
4. University of Essex, Colchester, UK.
5. ENEA-CNR, Padova, Italy.
6. Princeton Plasma Physics Laboratory, New Jersey, USA.
7. UKAEA Culham Laboratory, Abingdon, Oxon, UK.
8. Universidad Complutense de Madrid, Spain.
9. Institute of Mathematics, University of Oxford, UK.
10. Freien Universität, Berlin, F.R.G.
11. Swedish Energy Research Commission, S-10072 Stockholm, Sweden.
12. Imperial College of Science and Technology, University of London, UK.
13. Max Planck Institut für Plasmaphysik, Garching bei München, FRG.
14. Risø National Laboratory, Denmark.
15. FOM Instituut voor Plasmafysica, 3430 Be Nieuwegein, The Netherlands.
16. University of Lund, Sweden.
17. North Carolina State University, Raleigh, NC, USA
18. Institute for Aerospace Studies, University of Toronto, Downsview, Ontario, Canada.
19. University of Strathclyde, 107 Rottenrow, Glasgow, UK.
20. Nuclear Engineering Laboratory, Lapeenranta University, Finland.
21. CIEMAT, Madrid, Spain.
22. Institute for Nuclear Studies, Otwock-Swierk, Poland.
23. Kurchatov Institute of Atomic Energy, Moscow, USSR
24. University of Heidelberg, Heidelberg, FRG.
25. Institute for Mechanics, Academia Sinica, Beijing, P.R. China.
26. Southwestern University of Physics, Leshan, P.R. China.
27. RCC Cyfronet, Otwock Swierk, Poland.
28. JAERI, Naka Fusion Research Establishment, Ibaraki, Japan.
29. ENEA, Frascati, Italy.

At 1st June 1991